New aspects of bistatic SAR: processing and experiments

Joachim H. G. Ender, I. Walterscheid, Andreas R. Brenner
FGAN-FHR, Neuenahrer Str. 20, D-53343 Wachtberg, Germany
Tel: +49 228 9435-226, Fax: +49 228 9435-627, E-Mail: ender@fgan.de

***Abstract*— The interest in bistatic synthetic aperture radar, using separated transmitter and receiver flying on different platforms, has been increasing rapidly over the last years. The reason for this are specific advantages, like the reduced vulnerability in military systems, forward looking SAR imaging, additional information about the target, or increased RCS (see e.g. [1]). Nevertheless, besides technical problems (see [2]) - like the synchronisation of the oscillators, the involved adjustment of transmit pulse versus receive gate timing, antenna pointing, flight coordination, double trajectory measurement and motion compensation - the processing of bistatic radar data is still not sufficiently solved. Some of the possibilities and problems will be discussed. The second part of this paper deals with a bistatic experiment performed in November 2003: Two SAR systems of FGAN have been flown on two different airplanes, the AER-II system has been used as a transmitter and the PAMIR system as a receiver. Different spatially invariant flight geometries have been tested. High resolution bistatic SAR images were generated successfully.**

I. Introduction to bistatic SAR processing

There are different approaches to bistatic SAR processing based on well-known classes of monostatic processors with either high numerical effort or more or less tolerable approximations ([3] - [6]). Recently, in [7] a technique was introduced, how bistatic raw data can be transformed in such a way that a monostatic SAR processor can be applied. The key to this approach, the so called "Rocca's smile operator", has been further discussed in [8].

Bistatic SAR processing can be ordered on the one hand by the type of processor, on the other hand according to the flight situation. First, we recall the principle types of processors. The *matched filter processor* (MFP) optimises the signal-to-noise-ratio and offers an optimum but computationally inefficient solution. For each pixel of the image, the signal expected from a scatterer at this place is complex conjugated, multiplied by the measured data and summed up. The *local aperture optimum processor* (LAP) approximates the MFP for short apertures yielding an image of in principle non limited size, but with a coarse azimuth resolution. It tends to a simple *range-Doppler processor* without range migration correction, which starts with a range compression and then works along the range bins separately.

The idea of the range-Doppler processor including range migration compensation (RDP) can be transferred to the bistatic case. The *local image optimum processor* (LIP) approximates the MFP in a small region around an image point. It results in a generalised polar reformatting scheme. The *backprojection processor* (BPP) performs a successive image formation after range compression by projecting the range lines from the appropriate direction onto the image plane. The computational effort of this technique can be decreased by *fast backprojection processing* (FBP) techniques. One of the most popular techniques for the monostatic case is the *range migration processor* (RMP) combining near-optimum performance with high numerical efficiency. The key step of the RMP is formed by an interpolation in the k-space. An exact solution for an RMP in the bistatic case has not been presented up to now; nevertheless, [5] and [6] show how an approximate processor of this type can be evaluated. Finally, the pre-processing technique (PPT) ([7]) combined with any monostatic processor is a way to achieve focused bistatic SAR images.

To rank the complexity of the geometrical situation, we regard different stages ([6]): *Stage 0* describes the monostatic geometry (i. e. the simplest special case). *Stage 1* is called 'tandem configuration': Receiver and transmitter are travelling along the same path with constant and equal velocities. *Stage 2* denotes the 'translationally invariant configuration', i. e. receiver and transmitter have the same velocity vector. If the coordinates in the direction of motion coincide, the 'across track' situation is given. *Stage 3* describes the 'constant velocity configuration': Receiver and transmitter have arbitrary but constant velocity vectors, and *stage 4* refers to the general configuration with receiver and transmitter travelling along arbitrary flight paths. Further, we have to discriminate, if a strip-map type of an image is desired or a spotlight type, or if even a "sliding mode" is considered. This determines the beamsteering of the antennas, and effects time-invariant or time-variant data-windows in the azimuth-frequency region.

Not each of the above mentioned processors can be applied to each stage of geometrical complexity. For instance, the RMP introduced in [6] demands a translational invariant

0-7803-8742-2/04/$20.00 (C) 2004 IEEE

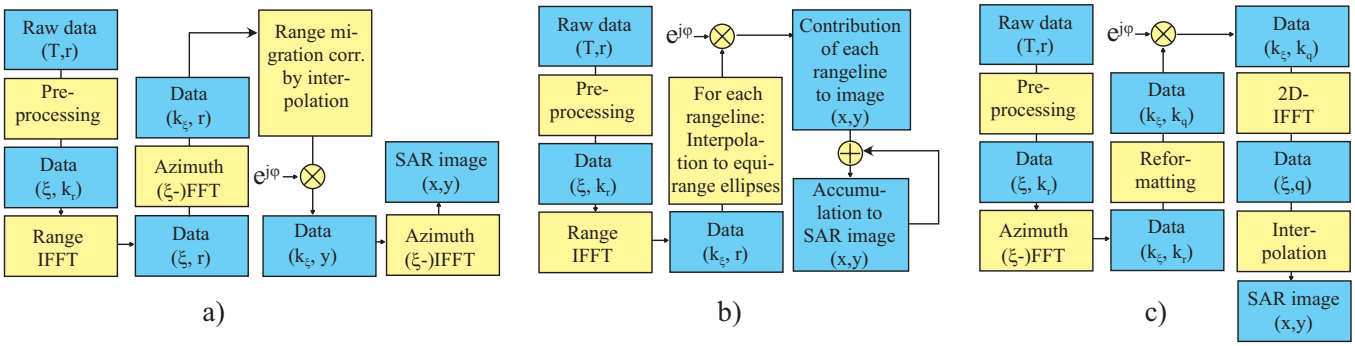

Fig. 1. Bistatic processors: a) Range-Doppler processor, b) Backprojection processor, c) Modified range-migration processor

configuration, the PPT in [7] even a pure tandem configuration.

II. Premises

Let the positions of the transmit and receive antenna phase centres be denoted by $\mathbf{R}_i(\xi)$, $i = 1, 2$, where ξ parametrises the paths of the two antennas. In the following, we assume that they are linear functions of ξ:

$$\mathbf{R}_i(\xi) = \mathbf{R}_i^{(0)} + \xi \mathbf{v}_i, \quad i = 1, 2 \tag{1}$$

($\mathbf{v}_i$ are the velocity vectors, if ξ is chosen to be the time). The arithmetic mean $\mathbf{R}_{mono}(\xi) = (\mathbf{R}_1(\xi) + \mathbf{R}_2(\xi))/2$ serves as a monostatic reference.

Further, we regard an arbitrary point scatterer at the position $\mathbf{r} = (x, y, z)^t$. We define the transmit and the receive range history of that point by $R_i(\xi; \mathbf{r}) = |\mathbf{R}_i(\xi) - \mathbf{r}|, \quad i = 1, 2$ and the bistatic range history by the sum $R(\xi; \mathbf{r}) = R_1(\xi; \mathbf{r}) + R_2(\xi; \mathbf{r})$. Some approaches to bistatic processors like [7] start from the range history due to the monostatic reference and compensate the difference of the bistatic range history.

After transformation of the recorded samples to the range wavenumber domain (denoted by k_r) and inverse filtering (see [15]) the signal from a point scatterer at position $\mathbf{r}$ with a normalized reflectivity is given by

$$s(\xi, k_r; \mathbf{r}) = e^{-jk_r R(\xi;\mathbf{r})} w(\xi; \mathbf{r}) \tag{2}$$

over the covered k_r-interval. The window $w(\xi, \mathbf{r})$ comprises the effect of the two antenna patterns and the radar range law. If the reflectivity distribution is denoted by $a(\mathbf{r})$, the signal of all scatterers is the superposition of the individual contributions:

$$z(\xi, k_r) = \int s(\xi, k_r; \mathbf{r}) a(\mathbf{r}) d\mathbf{r}. \tag{3}$$

The maximum SNR for a reconstruction of the reflectivity is achieved by the *matched filter processor*

$$\hat{a}(\mathbf{r}) = C \iint z(\xi, k_r) e^{jk_r R(\xi;\mathbf{r})} d\xi dk_r, \tag{4}$$

provided that the superposed noise is white over ξ and k_r.

III. Bistatic range-Doppler processor

A range-Doppler type processor has been applied to real bistatic data (see SAR image displayed in Fig. 4). It consists of the following steps (see Fig. 1, part a):

The data are pre-processed and the range-compression is performed. For the pre-processing, the knowledge of the transmitted waveform is necessary; either, a-priori assumptions can be applied, or the direct signal can be analysed, or the waveform can be extracted from the raw data, using strong point reflectors. Drifts of the receive-gates and the oscillators have to be compensated. The next step is an "azimuth"-FFT (better: ξ-FFT). Now, a Doppler- and range dependent range migration correction is performed by interpolation. The phase of the azimuth-signal has to be compensated. These two steps demand the precise knowledge of the flight paths, or an autofocus algorithm has to be applied. The processing is completed by an azimuth IFFT.

IV. Bistatic backprojection processor

According to Eq. 4, the integration along k_r can be performed for each ξ resulting in a range-compressed signal $Z(\xi, r)$. The second integral sums up all the contributions from the different points of the path:

$$\hat{a}(\mathbf{r}) = \int Z(\xi, R(\xi; \mathbf{r})) d\xi. \tag{5}$$

This integral can be carried out by adding from pulse to pulse the relating contributions from the range compressed signal for each pixel of the final image (see Fig. 1, part b). Since the data acquisition is done in the base-band, a phase compensation due to the bistatic range history has to be applied. The scene and the flight path are modelled in truly three-dimensional coordinates.

Of course, the pre-processing steps described in the former paragraph and autofocusing have to be performed, too. An image achieved by this processor for real data is shown in Fig. 5.

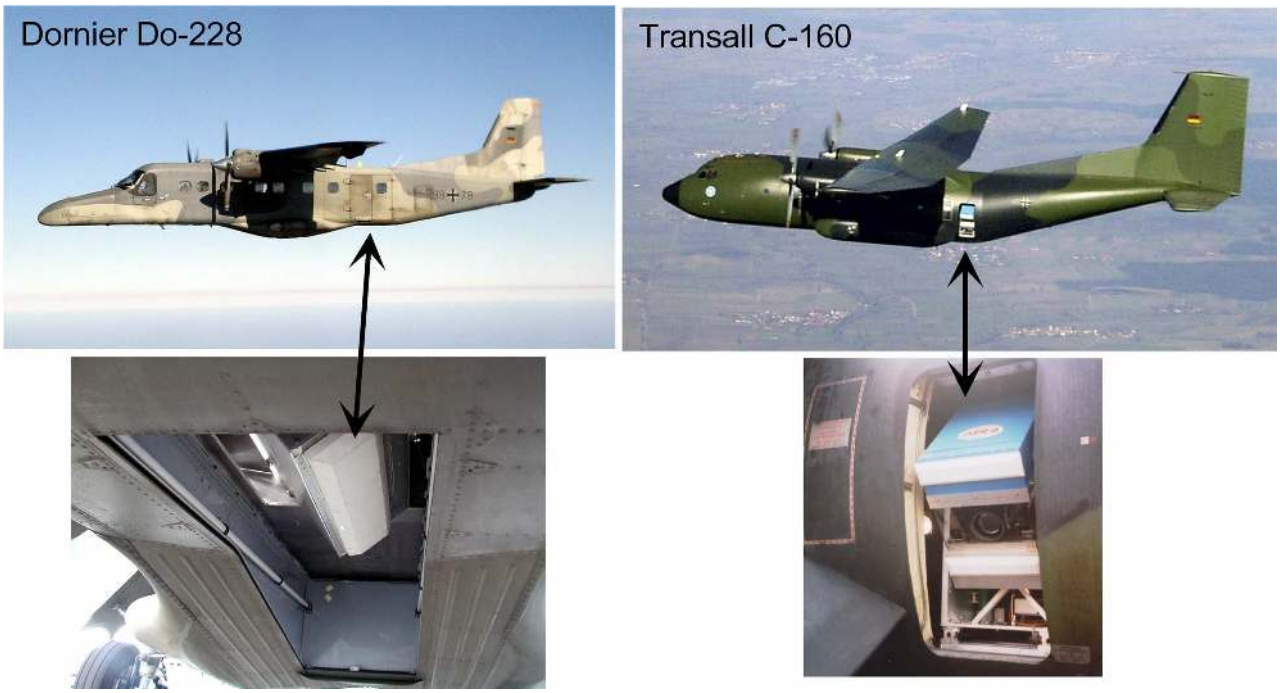

Fig. 2. Systems and carriers. Left: Dornier Do-228 with AER-II, right: Transall C-160 with PAMIR

V. Bistatic range migration processor

As a step to a numerically efficient processor we introduced a processor of a type characterised by "frequency-domain", "range-migration" or "omega-k" in [6]. The well known monostatic range migration processor transforms the data into the (k_ξ, k_r)-domain, followed by an interpolation ("Stolt interpolation") to the (k_ξ, k_y)-domain. An inverse 2D-Fourier transform results in the complex SAR image. For the bistatic case, this procedure cannot be applied directly. In the following, we restrict our considerations to the spatially invariant case. The idea of [6] is that an arbitrary deformation of the y-variable to a new q-variable is allowed. By the application of the principle of stationary phase, it can be shown that an exact processor of omega-k type results if the stationary phase

$$\Psi(k_r, C, q) = -k_r G(C, q), \tag{6}$$

where $C = -k_\xi / k_r$ is a generalised cosine, contains the linear function $G(C, q)$ of the new variable q for each C. It was shown that the monostatic geometry has this property for a certain choice of $y = f(q)$. In the general translationally invariant case, the stationary phase has to be evaluated numerically, and the function $G(C, q)$ has to be approximated by a linear fit.

The remaining errors can be controlled by dividing the frequency data into several segments which are processed separately. It should be mentioned, that our processor passes into the optimum processor for any of the following limits: a) swathwidth-to-range ratio tends to zero, b) bistatic angle tends to zero, c) relative bandwidth tends to zero.

The subsequent steps to be performed are:

- Transform data to the (k_x, k_r) - domain,
- Determine the mapping $y = f(q)$ in such a way that $G(C^*, q)$ is linear in q for a central C^*,
- For each C, q calculate $G(C, q)$. For each C, perform a MMS straight line fitting of $G(C, q)$ in the q-variable by $g(C) + h(C)q$,
- Develop the image in the (k_x, k_q)-domain by interpolation and multiplication by a phasor. Apply a two-dimensional inverse Fourier transform to the (x, q)-domain, Re-sample the image to the (x, y)-plane,
- Repeat the process for different segments, if the introduced phase error is too large.

VI. Flight experiments

Besides other European radar research institutes, like the DLR and ONERA [10], [11], or QinetiQ [12] the FGAN also undertook a bistatic airborne experiment with its two SAR sensors PAMIR and AER-II last year [13], [14]. The experiments consisted of several flight configurations with bistatic angles from 13 up to 76 degrees. To the authors' knowledge, these are the first experiments with such a large bistatic angle and a signal bandwidth of 300 MHz.

The transmitting sensor, AER-II, was placed on a Dornier Do-228 and the receiving sensor, PAMIR, on a Transall C-160 ([15], [16], [17]). Both SAR sensors operate at X-band and their bandwidths coincide over a range of 300 MHz. Due

Fig. 4. Images of part of an airfield. Left: bistatic SAR image, right: optical image

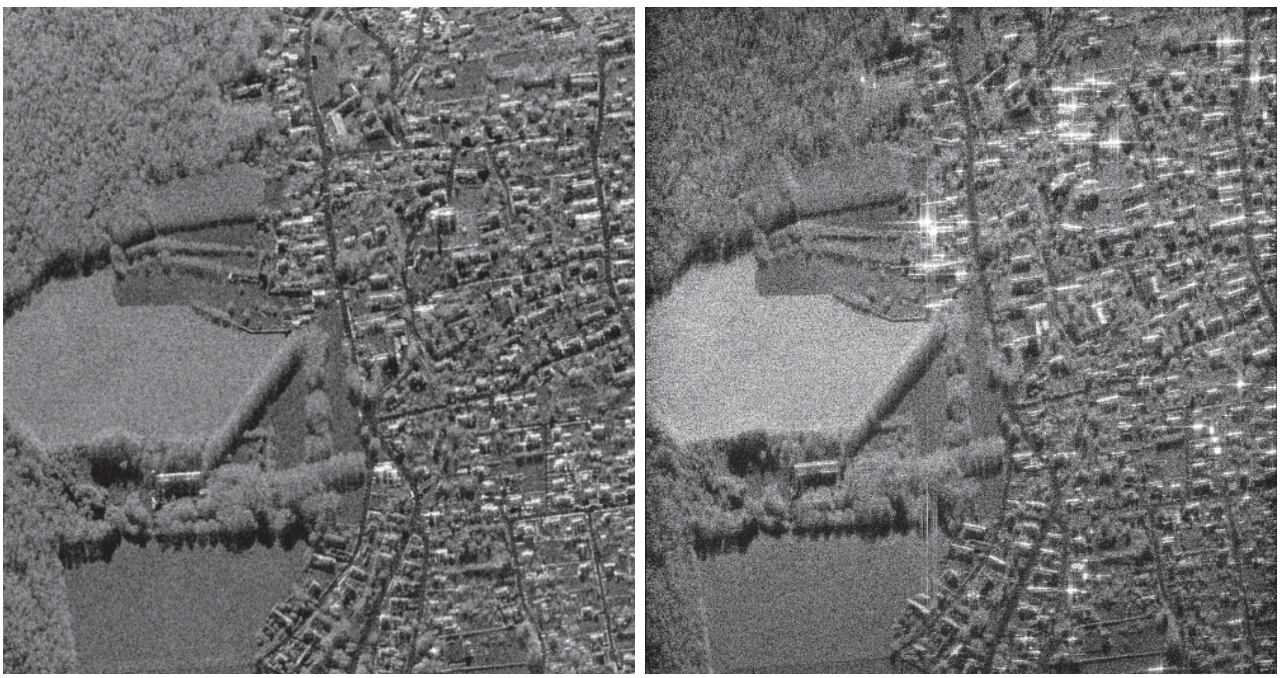

Fig. 5. Left: monostatic SAR image for comparison, right: bistatic SAR image of the same scene processed with the BPP

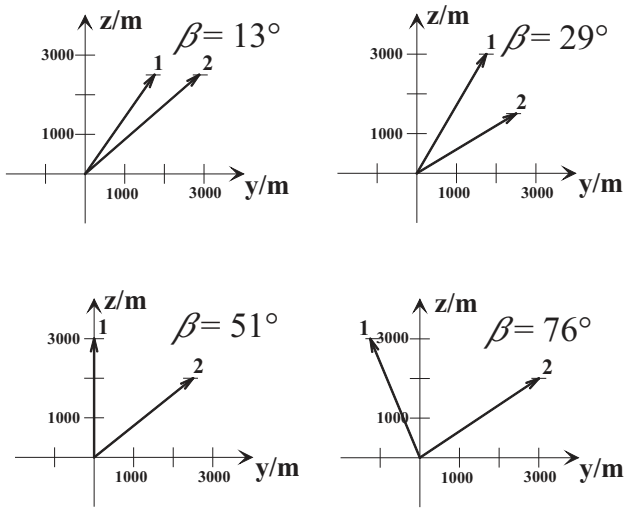

Fig. 3. Flight geometries used in the experiment (1=transmitter, 2=receiver)

to a large receiving window a synchronisation of the system oscillators was not necessary. In all flight configurations the two aircraft flew in the translationally invariant configuration. Primarily, the influence of the bistatic angle (see Fig. 3) was explored. For this purpose, the distance and the altitudes of the airplanes were adjusted in such a way that bistatic angles from 13 up to 76 degrees resulted.

First SAR images show the success of the bistatic flight campaign. The bistatic SAR image presented in Fig. 4 was recorded in a flight configuration with a bistatic angle of 29 degrees according to Fig. 3. The bistatic SAR image shows part of an airfield. At the top one can see the runway and some other taxiways, while at the bottom one can recognize two hangars. In order to evaluate the bistatic image, an optical image of the same scene is included.

The right image in Fig. 5 is processed using the bistatic backprojection algorithm. The flight configuration for this image differs from Fig. 4 in that the airplanes were flying at the same altitude with a bistatic angle of 13 degrees. On the left a monostatic image of the same scene is displayed.

VII. Summary

In this paper, three types of bistatic processors have been addressed. The first two of them, the bistatic range-Doppler processor and the bistatic backprojection processor were applied to real data collected during a flight campaign with the two SAR systems AER and PAMIR. The third, a new bistatic processor of omega-k type, has been introduced in [6] and was tested for simulated data. The next step will be to apply it to the measured data.

Acknowledgment

For the performance of the flight trials, we thank the technical center of the Bundeswehr WTD 61. This work is funded by the German Federal Ministry of Defense (BMVg) and the Federal Office of Defense Technology and Procurement (BWB).

References

[1] Krieger, G., Fiedler, H., Moreira, A.: "Bi- and Multi-Static SAR: Potetials and Challenges", European conference on synthetic aperture radar (EUSAR'04), Ulm, Germany, May 2004, pp. 365-370

[2] Cantalloube, H., Wendler, M., et al.: "Challenges in SAR processing for airborne bistatic acquisitions", European conference on synthetic aperture radar (EUSAR'04), Ulm, Germany, May 2004, pp. 577-580

[3] Soumekh, M.: "Wide-bandwidth continuous-wave monostatic/bistatic synthetic aperture radar imaging", International Conference on Image Processing, Chicago, Oct. 1998, pp, 361-364

[4] Ding, Y., Munson, D. C.: "A fast back-projection algorithm for bistatic SAR imaging", IEEE Intern. Conf. on Image Proc., Rochester, Sept 2002

[5] Ender, J.: "Signal Theoretical Aspects of Bistatic SAR", IEEE International Geoscience and Remote Sensing Symposium IGARSS'03, Tolouse, July 2003

[6] Ender, J.: "A step to bistatic SAR processing", European conference on synthetic aperture radar (EUSAR'04), Ulm, Germany, May 2004, pp. 359-364

[7] D'Aria, D., Monti Guarnieri, A., Rocca, F.: "Bistatic SAR Processing using Standard Monostatic Processor", European conference on synthetic aperture radar (EUSAR'04), Ulm, Germany, May 2004, pp. 385-388

[8] Loffeld, O., Nies, H., Gebhardt, U., Peters, V., Knedlik, S.: "Bistatic SAR - Some Reflections on Rocca's Smile...", European conference on synthetic aperture radar (EUSAR'04), Ulm, Germany, May 2004, pp. 379-384

[9] Ender, J.: "The meaning of k-space for classical and advanced SAR-techniques", PSIP'2001, Marseille, January 2001

[10] Wendler, M., Krieger, G., et al.: "Results of a Bistatic Airborne SAR Experiment", IRS 2003 Proc., Dresden, 2003, pp. 247-253

[11] Dubois-Fernandez, P., Cantalloube, H., et al.: "Analysis of bistatic behaviour of natural surfaces", European conference on synthetic aperture radar (EUSAR'04), Ulm, Germany, May 2004, pp. 573-576

[12] Yates, G., Horne, A.M., et al. "Bistatic SAR image formation", European conference on synthetic aperture radar (EUSAR'04), Ulm, Germany, May 2004, pp. 581-584

[13] Walterscheid, I., Brenner, A., Ender, J.: "Geometry and System Aspects for a Bistatic Airborne SAR-Experiment", European conference on synthetic aperture radar (EUSAR'04), Ulm, Germany, May 2004, pp. 567-570

[14] Walterscheid, I., Brenner, A., Ender, J.: "New Results on Bistatic Synthetic Aperture Radar", submitted to Electronic Letters

[15] Ender, J., Berens, P., et al.: "Multichannel SAR/MTI system development at FGAN: From AER to PAMIR", Proceedings of IGARSS'02, Toronto, Canada, 2002.

[16] Brenner, A., Ender, J.: "Very wideband radar imaging with the airborne SAR sensor PAMIR", Proceedings of IGARSS'03, Toulouse, France, 2003

[17] Brenner, A., Ender, J.: "Airborne SAR Imaging with Subdecimeter Resolution", European conference on synthetic aperture radar (EUSAR'04), Ulm, Germany, May 2004, pp. 267-270